Received: 16 July 2018 | Revised: 11 October 2018 | Accepted: 9 November 2018

DOI: 10.1002/mrm.27621

FULL PAPER

Magnetic Resonance in Medicine

# A unique anisotropic $R_2$ of collagen degeneration (ARCADE) mapping as an efficient alternative to composite relaxation metric ($R_2$-$R_{1\rho}$) in human knee cartilage study

Yuxi Pang[1] | Riann M. Palmieri-Smith[2,3] | Dariya I. Malyarenko[1] | Scott D. Swanson[1] | Thomas L. Chenevert[1]

[1]Department of Radiology, University of Michigan, Ann Arbor, Michigan

[2]School of Kinesiology, University of Michigan, Ann Arbor, Michigan

[3]Department of Orthopedic Surgery, University of Michigan, Ann Arbor, Michigan

**Correspondence**
Yuxi Pang, Department of Radiology, University of Michigan, 1500 E. Medical Center Drive, Ann Arbor, MI 48109-5030.
Email: yuxipang@umich.edu
Twitter: @yuxipang

**Purpose:** Anisotropic transverse $R_2$ ($1/T_2$) relaxation of water proton is sensitive to cartilage degenerative changes. The purpose is to develop an efficient method to extract this relaxation metric in clinical studies.

**Methods:** Anisotropic $R_2$ can be measured inefficiently by standard $R_2$ mapping after removing an isotropic contribution obtained from $R_{1\rho}$ mapping. In the proposed method, named as a unique anisotropic $R_2$ of collagen degeneration (ARCADE) mapping, an assumed uniform isotropic $R_2$ was estimated at magic angle locations in the deep cartilage, and an anisotropic $R_2$ was thus isolated in a single T2W sagittal image. Five human knees from 4 volunteers were studied with standard $R_2$ and $R_{1\rho}$ mappings at 3T, and anisotropic $R_2$ derived from ARCADE on the T2W (TE = 48.8 ms) image from $R_2$ mapping was compared with the composite relaxation ($R_2 - R_{1\rho}$) using statistical analysis including Student's t-test and Pearson's correlation coefficient.

**Results:** Anisotropic $R_2$ (1/s) from ARCADE was highly positively correlated with but not significantly different from standard $R_2 - R_{1\rho}$ (1/s) in the segmented deep ($r = 0.83 \pm 0.06$; $8.3 \pm 2.9$ vs. $7.3 \pm 1.9$, $P = .50$) and the superficial ($r = 0.82 \pm 0.05$; $3.5 \pm 2.4$ vs. $4.5 \pm 1.6$, $P = .39$) zones. However, after eliminating systematic errors by the normalization in terms of zonal contrast, anisotropic $R_2$ was significantly higher ($60.2 \pm 18.5\%$ vs. $38.4 \pm 16.6\%$, $P < .01$) than $R_2 - R_{1\rho}$ as predicted.

**Conclusion:** The proposed anisotropic $R_2$ mapping could be an efficient alternative to the conventional approach, holding great promise in providing both high-resolution morphological and more sensitive transverse relaxation imaging from a single T2W scan in a clinical setting.

**KEYWORDS**

anisotropic $R_2$, chemical exchange effect, composite relaxation metric $R_2 - R_{1\rho}$, human knee cartilage, magic angle effect

  

# 1 | INTRODUCTION

Water proton $T_1$ and $T_2$ relaxation times in pure liquids are primarily determined by modulation of the intramolecular dipole–dipole interaction created by molecular isotropic reorientation and characterized by a rotational correlation time $\tau_c$.[1] In biological tissue, magnetization transfer between water and immobilized components affects $T_1$ relaxation times, and water exchange between free and restricted domains alters $T_2$ relaxation times. In addition, intricate cellular and microstructural arrangements can restrict molecular reorientation of water, creating an orientation-dependent $T_2$ and $T_{1\rho}$ (spin-lattice relaxation time in a rotating frame) in highly organized tissues such as skeletal muscles and collagen fibers.[1-3] A simple method for quick quantification of MR anisotropic relaxation could provide invaluable insights into the integrity of structured tissues.

Articular cartilage primarily comprises water (~68-85% total weight), structural proteins including mostly collagen (60-80% dry weight) and proteoglycans (~15-40% dry weight), and a sparse distribution (~2%) of chondrocytes. Proteoglycans consist of a core with one or more negatively charged linear glycosaminoglycan (GAG) chains covalently attached. In contrast, collagen forms fibrils and fibers intertwined with proteoglycans.[4] Histologically, articular cartilage could be divided into the superficial (SZ), transitional (TZ), and deep (DZ) zones, where collagen fibers are, respectively, orientated in parallel, randomly, and perpendicularly with respect to the cartilage surface.[4-6] These highly organized collagen fibers, particularly in the DZ, create an anisotropic environment for the vast amount of water in cartilage, resulting in reported MR relaxation anisotropies.[1,7-9]

The orientation-dependent MR relaxation rates $R_1$ ($1/T_1$), $R_2$ ($1/T_2$), and $R_{1\rho}$ ($1/T_{1\rho}$) in bovine patellar cartilage–bone specimens have been recently characterized at 9.4T.[9] $R_{1\rho}$ was determined with both constant amplitude and adiabatic waveforms as a function of spin-lock RF power. This study shows that the relaxation rates $R_1$ and $R_2$ had minimal and maximal orientation dependences, respectively. The orientation anisotropy of $R_{1\rho}$ was almost completely suppressed if a stronger spin-lock RF field was used. More importantly, the relaxation parameters with higher orientation anisotropies were found to be more sensitive to cartilage degenerative changes secondary to osteoarthritis (OA). In other words, the anisotropic component of $R_2$ (i.e., $R_2^a(\theta)$) has the potential to be a more sensitive MRI biomarker for early cartilage changes in OA and a valuable imaging tool to follow OA progression after anterior cruciate ligament (ACL) reconstruction surgery.[10,11]

In conventional $R_2$ mapping, $R_2^a(\theta)$ is not separated from its isotropic counterpart, potentially compromising the sensitivity and specificity of the measure. $R_2$ and $R_{1\rho}$ are currently the most investigated relaxation metrics in clinical studies of knee cartilage degeneration,[11-13] but the interpretation of $R_2$ and $R_{1\rho}$ measurements in terms of observed structural protein changes is not straightforward.[12,14,15] Most likely, neither $R_2$ nor $R_{1\rho}$ has sufficient sensitivity to the underlying biochemical and physiological changes in cartilage. To increase the sensitivity of MR detection of OA, a composite relaxation metric, $R_2 - R_{1\rho}$, has been proposed.[16,17] Subtracting $R_{1\rho}$ from $R_2$ removes the isotropic contribution to $R_2$ to a certain extent if the spin-lock RF used in $R_{1\rho}$ mapping is not strong enough. Previous work has proposed that $R_{1\rho}$ is driven by exchange of hydroxyl protons in GAG with bulk water protons. This hypothesis seems consistent with exchange-driven mechanisms that determine $R_{1\rho}$[11,17,18] but conflicts with previous findings in cartilage.[9,14,15,19-23]

Chemical shift increases linearly with increasing magnetic field ($B_0$), and the relaxation rate $R_2$, due to exchange between protons with different chemical shifts, increases quadratically with $B_0$.[17,18,21] In contrast, the contribution from dipolar interaction to $R_2$ is mostly independent of $B_0$.[21,24] Provided that an increased $R_2$ at a higher $B_0$ could be attributed entirely to the chemical exchange effect, a comparison of $R_2$ at two different $B_0$ should shed light on the relative importance of two different relaxation mechanisms. Mlynarik et al. performed a detailed study on $R_2$ and $R_{1\rho}$ of human cartilage–bone specimens at 2.95T and 7.05T and concluded that the (residual) dipolar interaction was the dominant relaxation mechanism at $B_0 \leq 3T$.[21]

Later, two clinical studies on healthy human knee cartilage showed that $R_2$ at 7T was either close to[23] or 18% larger than[20] that at 3T, suggesting that the chemical exchange effect would have contributed less than 4% to $R_2$ if it had been measured at 3T. A similar finding was reported for $R_{1\rho}$ of healthy human knee cartilage, with less than 15% increase at 7T relative to 3T.[22] Furthermore, the chemical exchange effect on $R_2$ at 3T can be simulated using published parameters,[25] i.e., H2O of 88 [M], GAG of 0.3 [M], exchange rate of 1 kHz, and chemical shift of 1 ppm, and it turned out to be a negligible value of 0.05 (1/s) compared with the observed $R_2$ of about 30 (1/s).[20,23]

In this work, we first show theoretically that the $R_2^a(\theta)$ of cartilage at 3T was partially and inefficiently separated in the reported composite relaxation metric.[26] The prolonged image acquisition protocol and demanding pulse sequences standardization across different MR systems have prevented the reported method from being favorably accepted by the clinical community.[13,17] Hence, an efficient method is proposed here to derive $R_2^a(\theta)$ based on a single T2W sagittal image, by eliminating an assumed constant isotropic $R_2$ contribution derived from the magic angle locations in the deep cartilage. We refer to our new method as a unique Anisotropic $R_2$ of CollAgen DEgeneration (ARCADE) mapping to emphasize its straightforward association with the integrity of collagen fibers.[6,27] The derived femoral cartilage $R_2^a(\theta)$ values in five knees from four volunteers were compared with those of

$R_2 - R_{1\rho}$. Our comparable results demonstrate that the proposed ARCADE mapping could be an efficient alternative to the conventional approach, holding great promise in providing both high-resolution morphological and more sensitive $R_2^a(\theta)$ imaging from a single T2W scan in clinical studies on joint cartilage.

## 2 | THEORY

For knee cartilage water proton MR relaxation study at 3T, only the intramolecular dipolar interaction between two protons in water will be considered to interpret the observed MR relaxation rates of $R_1$, $R_2$, and $R_{1\rho}$.[21,24,28] In general, these relaxation rates could be characterized using a two-pool fast exchange model, i.e., rapid water exchange between the "free" and "bound" pools, and thus represented as the weighted averages of two pools,[24] as shown in Equation 1,

$$R_m = f_i * R_m^i + f_b * R_m^a(\theta) \tag{1}$$

with m = 1, 2 and $1\rho$; $f_i$ and $f_b$ the molecular fractions of water in the "free" and "bound" pools, with $f_i + f_b = 1$; $R_m^i$ and $R_m^a(\theta)$ the contributions from a fast isotropic and a slow anisotropic molecular reorientation,[24] which could be characterized, respectively, by a smaller effective isotropic correlation time ($\tau_f$) and a larger apparent isotropic correlation time ($\tau_b \gg \tau_f$). To simplify the discussion, $R_m^i$ and $R_m^a(\theta)$ can absorb corresponding $f_i$ and $f_b$, to denote the "apparent" relaxation rates in the following unless stated otherwise.

The molecular anisotropic reorientation of the "bound" water in cartilage can be characterized using an axially symmetric model, with a correlation time $\tau_\parallel$ assigned to one rotation about the symmetry axis along the collagen fiber, and another correlation time $\tau_\perp$ to the rotation about an axis perpendicular to the symmetry axis.[29] If $\tau_\parallel$ is set to $\tau_f$ and much smaller than $\tau_\perp$ (i.e. $\tau_\perp \gg \tau_\parallel$), corresponding to the "bound" water preferential alignments,[1,24,30] the effective correlation time $\tau_b$ of the "bound" water could be determined only by $\tau_\perp$[29] leading to $\tau_b \gg \tau_f$. This conclusion had been long before stated that the preferential alignments of water molecules could effectively have their otherwise-short correlation times amplified by many orders of magnitude.[31] Therefore, it would not be surprising to see a significantly larger $\tau_b$ for the restricted water in the "bound" pool.

$R_2^a(\theta)$ can be explicitly written as $R_2^a * (3cos^2\theta - 1)^2/4$, where $R_2^a$ denotes the maximum anisotropic relaxation rate and $\theta$ an angle subtending the dipolar interaction vector and the $B_0$ direction.[7,24,32] $R_2^a(\theta)$ reportedly could be effectively suppressed in $R_{1\rho}$ measurements if using a stronger ($\omega_1/2\pi > 2.0$ kHz) spin-lock RF strength.[9,19] Accordingly, an effective isotropic correlation time $\tau_b$ for the "bound" water could be estimated to be at least larger than $0.5/\omega_1$. On the other hand, the corresponding $\tau_f$ for the "free" water should be at least larger than $0.62/\omega_0$, given that $R_2 \gg R_1$.[31,33] The Larmor frequency is denoted by $\omega_0/2\pi$ and equal to 128 MHz at 3T.

According to the classical MR relaxation theories,[24,34] water proton relaxation rates of $R_1$, $R_2$, and $R_{1\rho}$ could be expressed in terms of an effective isotropic rotational correlation time $\tau_c$ using Equations 2-4, and profiled correspondingly at 3T in Figure 1,

$$R_1 = K\left\{\frac{\tau_c}{1+\omega_0^2\tau_c^2} + \frac{4\tau_c}{1+4\omega_0^2\tau_c^2}\right\} \tag{2}$$

$$R_2 = K\left\{\frac{3\tau_c}{2} + \frac{2.5\tau_c}{1+\omega_0^2\tau_c^2} + \frac{\tau_c}{1+4\omega_0^2\tau_c^2}\right\} \tag{3}$$

$$R_{1\rho} = K\left\{\frac{1.5\tau_c}{1+4\omega_1^2\tau_c^2} + \frac{2.5\tau_c}{1+\omega_0^2\tau_c^2} + \frac{\tau_c}{1+4\omega_0^2\tau_c^2}\right\} \tag{4}$$

where $K$ is a constant of $1.056 * 10^{10}$ ($s^{-2}$) assuming a distance of 1.59 (Å) between two proton nuclei in water.[1,24] If $\tau_c \ll 0.62/\omega_0$ (~$0.8 * 10^{-9}$ s), all relaxation rates will become $5K\tau_c$, which describes a scenario for water molecules rotating freely in nonviscous liquids.[31] In cartilage, however, water can attain a longer $\tau_c$, depending on both interactions with its neighboring macromolecules and their relative orientations to $B_0$.[31]

For the "free" water ($0.62/\omega_0 < \tau_f < 0.5/\omega_1$) in cartilage, $R_{1\rho}^i$ is equal to $R_2^i$, while $R_1^i$ becomes progressively smaller than $R_2^i$ as $\tau_f$ increases. Notably, $R_1^a$ for the "bound" water

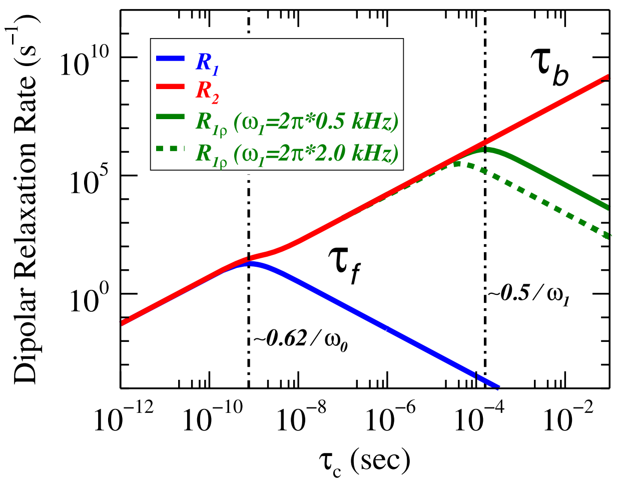


**FIGURE 1** Dependences of water proton dipolar relaxation rates (1/s) on an isotropic rotational correlation time $\tau_c$ (s) at 3T ($\omega_0/2\pi$ = 128 MHz), with $R_1$ and $R_2$ depicted, respectively, in blue and red solid lines, and $R_{1\rho}$ in green with $\omega_1/2\pi$ = 0.5 kHz (solid line), 2.0 kHz (dashed line). Effective correlation times in cartilage are represented by $\tau_f$ and $\tau_b$ for "free" and "bound" water, respectively

becomes insignificant, implying that the $R_1$ relaxation metric would be orientation-independent and only sensitive to the "free" water.[9,32,35,36] For the "bound" water ($\tau_b > 0.5/\omega_1$) in cartilage, $R_{1\rho}^a(\theta)$ is progressively decreased relative to $R_2^a(\theta)$ as $\tau_b$ grows. In this case, $R_{1\rho}^a(\theta)$ can be recast by $R_2^a(\theta) / \left(1+4\omega_1^2\tau_c^2\right)$ because of the dominant first term on the right side of Equations 3-4. It is worth mentioning that $R_{1\rho}$ will turn into $R_2$ (i.e. $R_2^i$+$R_2^a(\theta)$) and $R_2^i$, respectively, when a spin-lock RF is absent and a stronger ($\omega_1\tau_c \gg 0.5$) spin-lock RF is present. Consequently, the reported composite relaxation metric $R_2 - R_{1\rho}$ can be expressed in terms of $R_2^a(\theta)$ as shown in Equation 5, predicting that $R_2 - R_{1\rho}$ would be a partial $R_2^a(\theta)$ if a spin-lock RF strength is limited in clinical $R_{1\rho}$ mapping.[19,37]

$$R_2 - R_{1\rho} = R_2^a(\theta) * \left\{4\omega_1^2\tau_c^2 / \left(1+4\omega_1^2\tau_c^2\right)\right\} \quad (5)$$

Here, we propose an efficient alternative to derive $R_2^a(\theta)$ from one T2W sagittal image, assuming constant proton density ($S_0$) and $R_2^i$ in cartilage.[9,32,35] Typically, an orientation-dependent signal intensity $S(\theta)$ in T2W could be written as shown in Equation 6, including both "free" and "bound" water contributions, with TE being an echo-time.[6]

$$S(\theta) = S_0 \exp\left(-TE * R_2^i - TE * R_2^a(\theta)\right) \quad (6)$$

$$S(\theta = \pm 54.7°) = S_0 \exp\left(-TE * R_2^i\right) \quad (7)$$

$$R_2^a(\theta) = \{\log(S(\theta = \pm 54.7°)) - \log(S(\theta))\} / TE \quad (8)$$

As collagen fibers in the DZ are oriented predominately perpendicular to the cartilage surface,[6,32] $R_2^a(\theta)$ will become zero at the magic angles of ±54.7°.[7,8,32] In this case, Equation (6) will reduce to Equation (7), which represents the "free" water contribution as an internal reference of the assumed constant $S_0 \exp\left(-TE * R_2^i\right)$ in the deep cartilage. Combining Equation 6 and Equation 7, $R_2^a(\theta)$ could be easily computed using Equation (8). This proposed method has leveraged the specific femoral cartilage geometric information that can substitute the otherwise-required additional T2W measurement in conventional $R_2$ mapping.

## 3 | METHODS

### 3.1 | Volunteer subjects

Four volunteers (V1-V4) were enrolled in this study. The first three had a single knee scanned, while V4 had both knees scanned. Thus, five datasets (S1-S5) were generated and labeled accordingly by the volunteer's sex (M/F), age, and knee (L/R) health status (symptomatic [S], asymptomatic [A], or ACL repaired [P]), e.g., V4F20LP in Tables 1 and 2. This study was approved by the local institutional review board (IRB) and compliant with the Health Insurance Portability and Accountability Act (HIPAA). Each volunteer was informed about the study and signed a consent form.

### 3.2 | The MR imaging protocols

$R_2$ and $R_{1\rho}$ mappings were performed on a 3T MR scanner using a dedicated 16-Channel T/R Knee Coil. The 3D images with different spin-echo times (TEs) or spin-lock durations (TSLs) were acquired in the sagittal plane. An acceleration factor of 2 was used in fast parallel imaging.

*$R_2$ mapping*: An interleaved multislice (= 43) multiecho (= 8) turbo spin-echo pulse sequence was used in image acquisitions with a voxel size of 0.6 * 0.6 * 3.0 mm$^3$ and a field of view of 128 * 128 * 128 mm$^3$ covering entire tibiofemoral compartments.[10] The reconstructed images were then interpolated to a voxel size of 0.24 * 0.24 * 3.00 mm$^3$. An effective TE for volumetric image data of each was n * 6.1 ms, with n = 1, 2, 3, 4, 5, 6, 7, 8. The pulse repetition time was 2500 ms, and the total scan time was about 9 minutes per knee.

*$R_{1\rho}$ mapping*: A spin-lock-prepared T1-enhanced 3D turbo gradient-echo sequence was used to acquire T1$\rho$ -weighed images through a segmented elliptic-centric k-space acquisition.[38] The spin-lock RF field strength ($\omega_1/2\pi$) was 0.5 kHz, and TSL was 0, 10, 20, 30, and 40 ms, respectively. A similar field of view was used with an acquired voxel size of 0.40*0.40*3.00 mm$^3$ (interpolated to 0.24*0.24*3.00 mm$^3$). The total scan time was about 11 minutes per knee.

**TABLE 1** Average relaxation rates (1/s) and Pearson correlation coefficients (*r*) from five femoral cartilages in the deep zone

| ID | Subject | $R_2$ | $R_{1\rho}$ | r | $R_2 - R_{1\rho}$ | $R_2^a(\theta)$ | r |
|---|---|---|---|---|---|---|---|
| S1 | V1M52RA | 24.2 ± 6.8 | 15.6 ± 3.3 | 0.39 | 8.6 ± 6.3 | 4.7 ± 6.7 | 0.83 |
| S2 | V2M47LS | 19.9 ± 6.8 | 14.7 ± 3.7 | 0.16 | 5.2 ± 7.2 | 5.9 ± 7.7 | 0.86 |
| S3 | V3F41LA | 20.8 ± 6.7 | 15.6 ± 3.1 | 0.25 | 5.3 ± 6.6 | 9.2 ± 7.9 | 0.75 |
| S4 | V4F20LP | 22.7 ± 8.5 | 13.5 ± 2.7 | 0.54 | 9.2 ± 7.4 | 11.5 ± 9.0 | 0.91 |
| S5 | V4F20RA | 24.6 ± 8.9 | 16.5 ± 4.1 | 0.32 | 8.1 ± 8.5 | 10.1 ± 8.2 | 0.79 |

*Note*. Relaxation rate is mean ± standard deviation. *P* value < .001 for all correlation coefficients.

**TABLE 2** Average relaxation rates (1/s) and Pearson correlation coefficients (r) from five femoral cartilages in the superficial zone

| ID | Subject | $R_2$ | $R_{1\rho}$ | r | $R_2 - R_{1\rho}$ | $R_2^a(\theta)$ | r |
|---|---|---|---|---|---|---|---|
| S1 | V1M52RA | 21.7 ± 6.6 | 15.7 ± 2.9 | 0.34 | 6.0 ± 6.3 | 1.6 ± 8.1 | 0.87 |
| S2 | V2M47LS | 16.0 ± 5.8 | 14.0 ± 3.7 | 0.50 | 2.0 ± 5.0 | 1.0 ± 7.2 | 0.76 |
| S3 | V3F41LA | 19.1 ± 7.7 | 14.7 ± 3.0 | 0.15 | 4.3 ± 7.9 | 5.8 ± 9.6 | 0.87 |
| S4 | V4F20LP | 18.5 ± 5.4 | 12.6 ± 2.3 | 0.44 | 5.8 ± 4.9 | 6.3 ± 5.9 | 0.84 |
| S5 | V4F20RA | 19.2 ± 6.2 | 14.8 ± 3.3 | 0.28 | 4.4 ± 6.2 | 3.1 ± 7.0 | 0.78 |

*Note*. Relaxation rate is mean ± standard deviation. $P$ value < .001 for all correlation coefficients.

## 3.3 | The MR image post processing

All data analysis and image visualization were performed using an in-house software developed in IDL 8.5 (Harris Geospatial Solutions, Inc., Broomfield, CO).

*Image coregistrations:* A free software *Elastix*[39] was used for intraseries and interseries image coregistrations. The T2W or T1$\rho$ 3D images with different TE and TSL were first aligned within time series; then, the aligned T1$\rho$ 3D images were further coregistered to the aligned T2W 3D images. The coregistration scheme was based on a published protocol for human knee cartilage, including a multiresolution approach and a rigid transformation model.[40] The coregistration was optimized over 1,000 iterations using a localized mutual information (MI) as a similarity metric, and mutual information was progressively maximized by minimizing its negative values in the optimization processes. The detailed coregistration parameter settings (par0017) can be found in http://elastix.bigr.nl/wiki.

*Angular-radial segmentation*: First, a whole femoral cartilage was manually delineated using a free software ITK-SNAP[41] for each image slice in T2W and T1$\rho$ 3D data. Region of interest (ROI) vertices were placed along cartilage boundaries, with the vertex path defined as smoothly as possible. Furthermore, nonoverlaid cartilage areas (due to motion or misalignment) in both T2W and T1$\rho$ images were minimized in delineating cartilage ROI. Second, the localized cartilage partitions were accomplished by an angular and radial segmentation method.[42] Specifically, the vertices (x and y coordinates) from a predefined cartilage ROI were used to fit (by a nonlinear least-squares fitting) a virtual circle in each image slice, with the circle center located in the femoral condyle.[42] Relative to a vertical line, an angle $\varphi$ of a "spoke" connecting each vertex and the circle center could be calculated; subsequently, the whole cartilage was subdivided angularly into 5$^\circ$ partitions based on the range of calculated "spoke" angles. A reference angle (0$^\circ$) was chosen as the $B_0$ direction in a sagittal image, with negative angles pointing to the anterior direction and the positive angles to the posterior direction, as shown in Figure 2. Third, as the shape of femoral cartilage deviates from an ideal half-circle, especially on the lateral sides,[43] a segmented angle $\varphi$ had to be recomputed using only adjacent ($\varphi \pm 10°$) vertices to generate a new angle $\theta$ to represent collagen fiber orientation closely in the deep cartilage. Finally, the femoral cartilage was further subdivided radially into the DZ and SZ, with a shared border line equidistant to opposite boundaries. This segmented SZ covers at least both the histologically defined the SZ and TZ.[4,5]

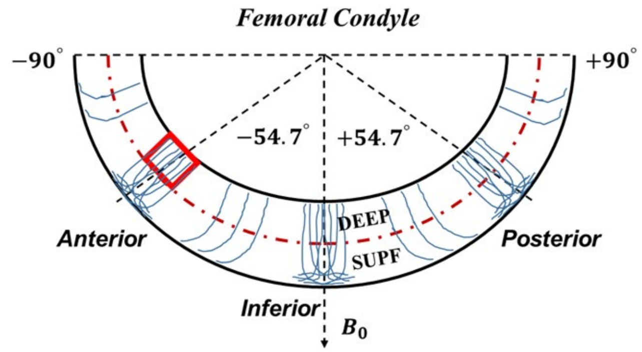


**FIGURE 2** A schematic diagram of femoral articular cartilage showing an angular-radial segmentation, anatomical annotations, and collagen fiber characteristic orientations. The deep and the superficial zones are divided by a red dash-dot line. A segmented region of interest (ROI), at a magic angle of −54.7° with an angular width of 5° in the deep zone, is highlighted by a red square. The main magnetic field $B_0$ points downward

*$R_2$-$R_{1\rho}$ parametric map:* Both $R_2$ and $R_{1\rho}$ parametric maps were fitted pixel-by-pixel from coregistered multiple 3D data based on a simple exponential relaxation decay model, i.e., $S(t_i) = S_0 \exp(-t_i * P)$, where $P = R_2$ or $R_{1\rho}$, and $t_i =$ [6.1, 12.2, 18.3, 24.4, 30.5, 36.6, 42.7, 48.8] or [0, 10, 20, 30, 40] (ms), respectively. The corresponding parametric error maps were also created by adjusting fitted parameter uncertainties so that the reduced $\chi^2$ was equal to 1.[44]

*$R_2^a(\theta)$ parametric map from ARCADE:* A single T2W (TE = 48.8 ms) 3D dataset from $R_2$ mapping was used. An internal reference corresponding to the "free" water contribution for each image slice was estimated using Equation 6. Specifically, the average T2W pixel values (in logarithmic scale) within each of segmented ROIs in the DZ were fitted to a function of collagen fiber orientations ($\theta$) as shown in Equation 9, with parametric bound constraints.

$$y = A - B * \left(3cos^2(\theta + C) - 1\right)^2 \quad (9)$$

The model parameter A was not constrained; however, B and C were limited to the ranges of [0, 10] and [−10°, +10°], respectively. The limited freedom introduced for $\theta$ was to account for potential systematic errors in collagen fiber orientations.[5,9]

The nonlinear curve fitting was performed slice by slice.[44] The optimal fits were determined using goodness of fits characterized by $\chi^2$ test statistics with a significant level of $P > .95$. Finally, the mean of those determined optimal A values was used as a global internal reference, i.e., $\log(S(\theta = 54.7°))$ in Equation (8).

*Statistical analysis*: The differences and associations between two relaxation metrics were, respectively, quantified using a Student paired t test (a two-tailed distribution) and a Pearson correlation coefficient ($r$), where the statistical significance was considered at $P < .05$. Scatterplots were used to demonstrate the potential correlation between two parameters; additionally, data ellipses with a 95% confidence level were included for visual enhancement.[45] A normalized relaxation metric, in terms of zonal contrast, was generated as $(DEEP - SUPF)/DEEP * 100\%$, with $DEEP$ and $SUPF$ representing $R_2^a(\theta)$ or $R_2 - R_{1\rho}$ in the DZ and SZ, respectively. All measurements are shown as mean ± SD unless stated otherwise.

## 4 | RESULTS

A half-circle femoral cartilage sketch is shown in Figure 2 to illustrate an angular-radial segmentation in a sagittal image, with a highlighted ROI (red square) at a magic-angle orientation in the DZ.

Figure 3 presents two segmentations (Figure 3A, C) from an exemplary dataset S4, and comparisons between segmented angles $\varphi$ and locally refined angles $\theta$ in one lateral image slice 14 (Figure 3A, B) and one medial image slice 23 (Figure 3C, D) from the left knee. Significant larger angle differences (11.0 ± 6.7° vs. 4.3 ± 3.4°, $P < .001$) were observed in the medial than those in the lateral side for these two image slices. Specifically, $\varphi$ in Figure 3D was overestimated ($|\varphi| > |\theta|$) and underestimated ($\varphi < \theta$) in the most anterior and posterior directions, respectively.

An internal reference determination for the same dataset in ARCADE mapping is demonstrated in Figure 4. A whole deep cartilage T2W map (in logarithmic scale) was generated (Figure 4A) based on segmented ROIs, where the segmented angles $\varphi$ of ±54.7° are indicated by two white dashed lines. An optimal (Figure 4B, $P = .998$) fit and a rejected (Figure 4C, $P = .052$) fit based on the refined angle $\theta$ are shown for the image slices 14 (as shown in Figure 3A) and 23 (as shown in Figure 3B), with their spatial locations highlighted by a white and a red arrow in the T2W map. For this femoral cartilage, the internal reference was determined as 5.757 ± 0.024.

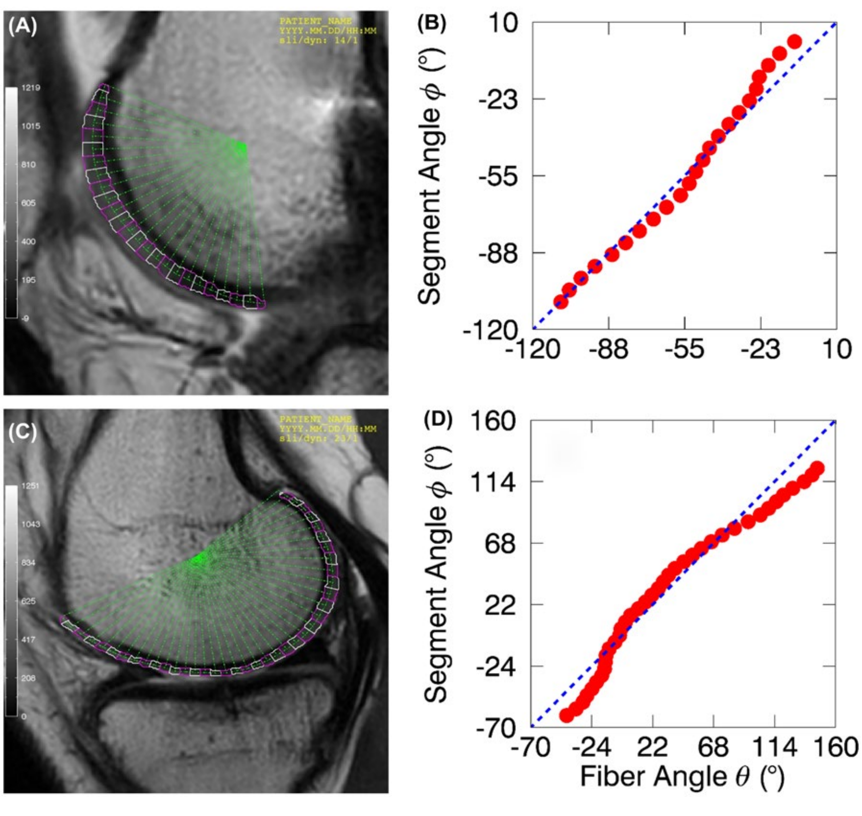


**FIGURE 3** Two examples of the angular-radial segmentation on a lateral image slice 14 (A) and a medial image slice 23 (C) from dataset S4, and a comparison between segmented angles ($\varphi$) and locally refined angles ($\theta$) for the image slice 14 (A, B) and the image slice 23 (C, D)

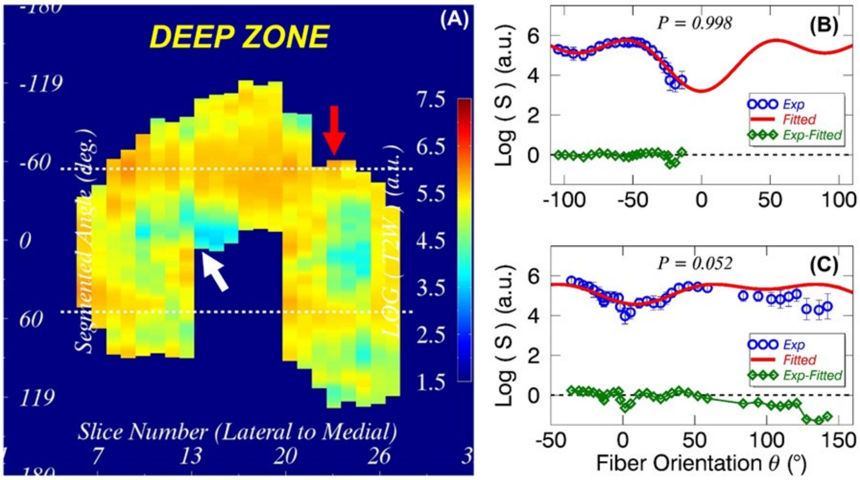


**FIGURE 4** An estimation of the isotropic relaxation contribution to T2W (in logarithmic scale) signal in the deep zone for dataset S4 (A). Examples of an optimal (B) fit and a rejected (C) fit for the image slices 14 (white arrow) and 23 (red arrow) as shown in T2W map (A), with two white dashed lines indicating the segmented angles $\varphi$ of ±54.7°

For the image slice 14 as shown in both Figures 3A and 5F, the derived pixel maps of $R_2$ (Figure 5A), $R_{1\rho}$ (Figure 5B), $R_2-R_{1\rho}$ (Figure 5D), and $R_2^a(\theta)$ (Figure 5E), along with the ROI-based profile comparisons among $R_2$, $R_{1\rho}$, $R_2-R_{1\rho}$ and $R_2^a(\theta)$ (Figure 5C), are presented in Figure 5. The observed orientation anisotropy of $R_{1\rho}$, compared with $R_2$, was significantly suppressed with a spin-lock RF strength ($\omega_1/2\pi$) of 500 Hz (Figure 5A-C). Noticeably, $R_2^a(\theta)$ was well aligned with the composite relaxation metric features with increased values and less image blurring (Figure 5C-E). The image acquisition time for ARCADE mapping in Figure 5E was significantly shorter than that for the composite relaxation metric as shown in Figure 5D (i.e., 1.2 vs. 20 minutes). The T2W image shown in Figure 5F had an echo time of 48.8 ms.

For the same dataset S4, Figure 6 presents the whole knee relaxation parametric maps of $R_2$ (Figure 6A, E), $R_{1\rho}$ (Figure 6B, F), $R_2-R_{1\rho}$ (Figure 6C, G), and $R_2^a(\theta)$ (Figure 6D, H) for the DZ (Figure 6A-D) and the SZ (Figure 6E-H). Qualitatively, all relaxation rates in the DZ were marginally larger than those in the SZ as previously reported, and $R_2^a(\theta)$ was comparable to $R_2-R_{1\rho}$.

Scatterplots of $R_2$ versus $R_{1\rho}$ (Figure 7A) and $R_2^a(\theta)$ versus $R_2-R_{1\rho}$ (Figure 7B) are shown in Figure 7 for quantitative evaluations, with data ellipses overlaid to enhance visualization of existing linear correlations. On average, $R_2$ (1/s) values and their variations were larger than those of $R_{1\rho}$ (1/s) in both the DZ (22.7 ± 8.5 vs. 13.5 ± 2.7) and the SZ (18.5 ± 5.4 vs. 12.6 ± 2.3). In contrast, $R_2^a(\theta)$ (1/s) values and their variances were only marginally larger than those of $R_2-R_{1\rho}$ (1/s) (i.e. 11.5 ± 9.0 vs. 9.2 ± 7.4 and 6.3 ± 5.9 vs. 5.8 ± 4.9) in these two zones. Unlike the weak associations between $R_2$ and $R_{1\rho}$ ($r$ = 0.54, 0.44, $P$ < .01, 0.01), $R_2^a(\theta)$ was highly positively correlated with $R_2-R_{1\rho}$ ($r$ = 0.91, 0.84, $P$ < .01, 0.01) in both segmented cartilage zones.

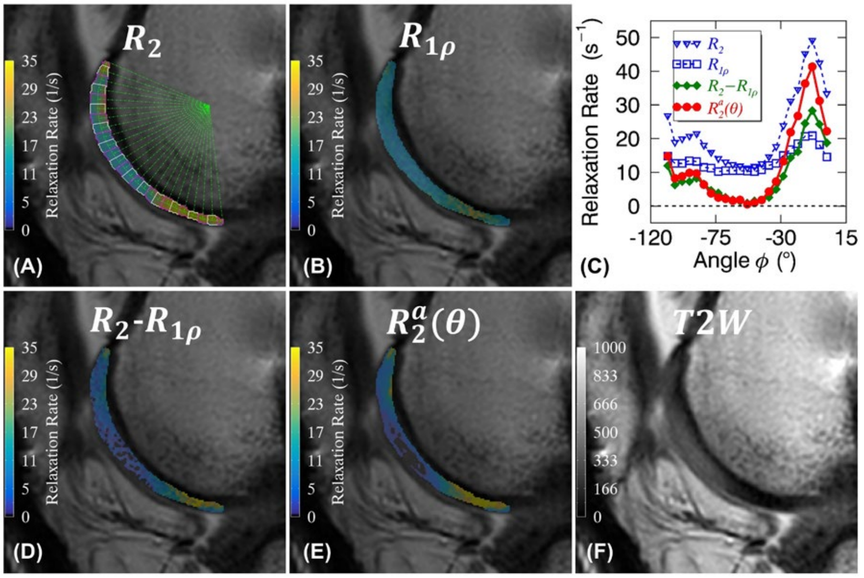


**FIGURE 5** Relaxation rate (1/s) pixel maps of $R_2$ (A), $R_{1\rho}$, (B), $R_2-R_{1\rho}$ (D), and $R_2^a(\theta)$ (E) for the image slice 14 (from dataset S4) as shown in (F). Derived from the average value within each of the segmented regions of interest (ROIs) as depicted in (A), the orientation-dependent profiles of $R_2$ (blue triangle), $R_{1\rho}$ (blue square), $R_2-R_{1\rho}$ (green diamond), and $R_2^a(\theta)$ (red circle) were compared in (C). The echo time (TE) was 48.8 ms for the T2W image shown in (F)

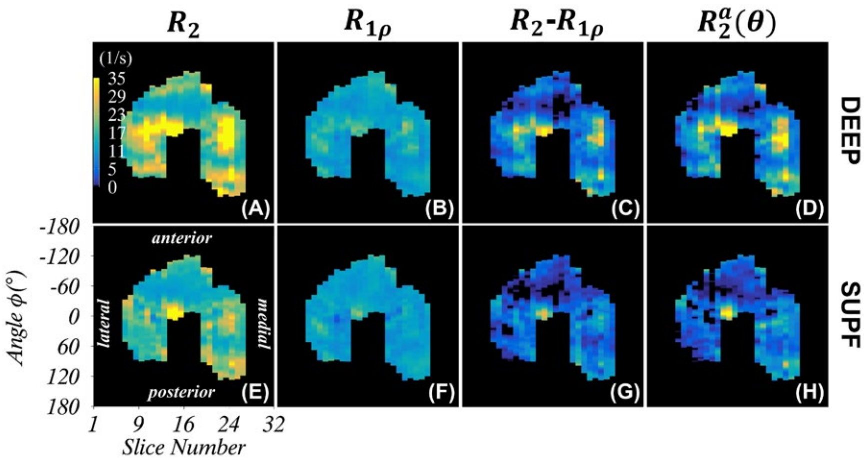


**FIGURE 6** Whole femoral cartilage region of interest (ROI)-based relaxation rate (1/s) maps of $R_2$ (A, E), $R_{1\rho}$ (B, F), $R_2-R_{1\rho}$ (C, G), and $R_2^a(\theta)$ (D, H) in the deep (A-D) and the superficial (E-H) zones for dataset S4. The slice number and the segmented angle $\varphi$ increase, respectively, from left (lateral) to right (medial) and up (anterior) to down (posterior). All figures are in the same color scale with the background set to zero (black)

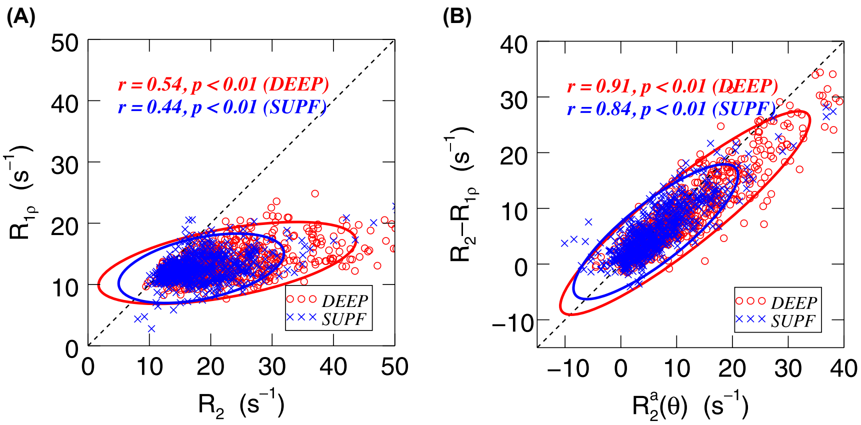


**FIGURE 7** Scatterplots of relaxation rates (1/s) of $R_2$ vs. $R_{1\rho}$ (A) and of $R_2^a(\theta)$ vs. $R_2-R_{1\rho}$ (B) in the deep (red circle) and the superficial (blue cross) zones with each data ellipse superimposed for dataset S4. The Pearson correlation coefficients ($r$) are included in the plots

The average relaxation rates and linear correlation coefficients from each cartilage in the DZ and the SZ are listed in Tables 1 and 2 for five examined knees. These tabulated values from the DZ are plotted against those in the SZ as shown in Figure 8A. The grand means of the average relaxation rates for five knees are represented by each data ellipse centroid. In general, $R_2$ (1/s) was significantly larger than $R_{1\rho}$ (1/s) in the DZ (22.4 ± 2.0 vs. 15.2 ± 1.1, $P < .01$) and the SZ (18.9 ± 2.0 vs. 14.4 ± 1.1, $P < .01$). $R_2^a(\theta)$ (1/s) was hardly distinguishable from $R_2-R_{1\rho}$ (1/s) in the DZ (8.3 ± 2.9 vs. 7.3 ± 1.9, $P = .50$) and the SZ (3.5 ± 2.4 vs. 4.5 ± 1.6, $P = .39$). However, the normalized $R_2^a(\theta)$, in terms of the zonal difference in cartilage, was significantly larger than the normalized $R_2-R_{1\rho}$ (i.e. 60.2 ± 18.5% vs. 38.4 ± 16.6%, $P < .01$) as shown in Figure 8B.

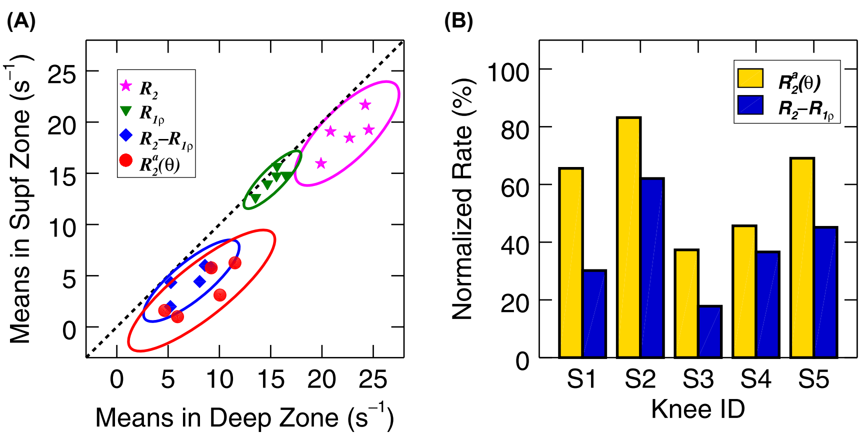


**FIGURE 8** A scatterplot of the means of relaxation rates (1/s) of $R_2$ (magenta star), $R_{1\rho}$ (green triangle), $R_2-R_{1\rho}$ (blue diamond), and $R_2^a(\theta)$ (red circle) in the deep zone against those in the superficial zone (A) with subgroup data ellipse superimposed, and a comparison between normalized $R_2^a(\theta)$ (yellow) and normalized $R_2-R_{1\rho}$ (blue) for five knees (B)

## 5 | DISCUSSION

In this work, we first established that the composite relaxation metric ($R_2 - R_{1\rho}$) actually measures inefficiently a partial anisotropic $R_2$ ($R_2^a(\theta)$) in clinical knee cartilage studies at 3T, and then introduced a new method to extract an uncompromised $R_2^a(\theta)$ based on a single T2W sagittal image. The comparable results between the derived $R_2^a(\theta)$ and the measured $R_2 - R_{1\rho}$ on five femoral cartilages demonstrated that the developed method could be an efficient alternative to the conventional approach.

A key assumption in the new method was a uniform proton density $S_0$ and a constant isotropic $R_2$ ($R_2^i$) regardless of its locations and health status in articular cartilage, where the differences in observed $R_2$ relaxation rates stemmed solely from the "bound" water on differently orientated collagen fibers. This oversimplified view on the "free" water was mainly based on previous observations in that the estimated water content and the observed $R_2$ values at the magic angle (MA) orientations were all nearly uniform across different zones in cartilage.[5,9,35,36,46]

For example, one *ex vivo* study showed that $S_0$ was marginally larger in the SZ than in the DZ (i.e. 90 ± 3% vs. 88 ± 4%) at a location near the MA.[46] Xia reported an approximately constant $T_2$ (59 ± 6 ms) in cartilage specimens when orientated at the MA in a high-resolution µMRI study.[5] He also found that $T_1$ was orientation-independent and almost constant (1.72 ± 0.11 sec), as was confirmed recently by Hänninen et al.[9] Based on MR relaxation theories, both isotropic $R_2^i$ and $R_1^i$ have nearly linear relationships albeit opposite with an effective correlation time $\tau_f$ of the "free" water in tissue. Thus, a uniform $R_1$ could be reasonably interpreted as a constant $R_2^i$, as the observed $R_1$ in cartilage is predominantly contributed from $R_1^i$.

As articular cartilage has a similar biochemical composition and structural network in extracellular matrix, the "free" water contribution to $R_2$ should not substantially fluctuate in different cartilages; in other words, the internal reference derived from the deep femoral cartilage is applicable to the tibial and patellar cartilages as well. Our preliminary data (not shown) indicated that comparable correlations between $R_2^a(\theta)$ and $R_2 - R_{1\rho}$ were found in the femoral, tibial, and patellar cartilages, and an average $R_2^a(\theta)$ in the tibial was almost three times larger than those found in the femoral and patellar cartilages.

The assumption used in ARCADE is no exception for an OA population. The integrity of collagen fibers could be compromised as a result of pathology leading to less preferentially orientated water, and the amount of released "free" water would be very small compared to an existing large pool of free water. Although the free water contribution to T2W signal should not be altered in OA subjects, the observed $T_2$ at the locations other than the MA orientations could be increased and could adversely impact optimal curve fittings in some image slices and thus potentially lead to a biased internal reference. On the other hand, if localized OA happens to be at the MA sites, the internal reference would not be altered unless an insignificant (<4% at 3T) chemical exchange effect associated with GAG loss were taken into account.

Had the assumption been violated, the derived $R_2^a(\theta)$ would have been offset systematically from its true value as the $R_2^a(\theta)$ computation was just a simple subtraction in logarithmic scale. In this work, the measured $R_2 - R_{1\rho}$ was expected to be smaller than $R_2^a(\theta)$ because of a limited spin-lock RF strength used in $R_{1\rho}$ mapping. According to previous reports,[9,19] a spin-lock RF strength of 2.0 kHz could adequately (let's say 99%) suppress $R_2^a(\theta)$, leading to $R_2 - R_{1\rho} = 99\%{*}R_2^a(\theta)$. In clinical $R_{1\rho}$ studies at 3T, however, the spin-lock RF strength is usually limited to 0.5 kHz,[37] which would translate into $R_2 - R_{1\rho} \approx 86\%{*}R_2^a(\theta)$. On the other hand, the observed $R_2 - R_{1\rho}$ could be erroneously increased due to different data acquisitions,[12,13,47] where $R_2$ derived from a multiecho pulse sequence tends to be more overestimated than $R_{1\rho}$ from a pulse sequence similar to 3D-MAPSS.[47] Consequently, the enhanced $R_2 - R_{1\rho}$ could compensate for the loss due to a limited spin-lock RF power, which might justify the comparable $R_2^a(\theta)$ and $R_2 - R_{1\rho}$ observed for some subjects in the current study.

Our derived $R_2^a(\theta)$ values generally agreed with the prediction in the DZ except for the first knee (S1). It was quite likely that the determined internal references for S1 in the DZ and for others in the SZ were underestimated, leading to an unexpected smaller $R_2^a(\theta)$. However, when using a normalized relaxation metric in terms of zonal contrast such as shown in Figure 8B, all systematic errors associated with the internal reference and pulse sequences became irrelevant, and the derived normalized $R_2^a(\theta)$ from ARCADE was significantly larger than the normalized $R_2 - R_{1\rho}$ as predicted. Furthermore, the observed variations in both $R_2^a(\theta)$ and $R_2 - R_{1\rho}$ (Tables 1 and 2, Figure 8A, B) might reflect collagen fiber unique arrangements due to the volunteers' different ages (20-52 yr), sexes (M/F), and knee health statuses (ACL repaired, asymptomatic, or symptomatic). Even though their true relaxation rates might be systematically offset, the reported significant correlations should not be impaired.

These encouraging comparable results alone would probably not be sufficient to justify an alternative to an established method. However, the great reduction in scan time required for clinical MR studies and the straightforward image post processing provide a strong impetus for further validating our new method in a large clinical study. Additionally, the quality of derived relaxation metric map from ARCADE could be much better as can be appreciated in the $R_2^a(\theta)$ pixel map

(Figure 5E) with respect to $R_2 - R_{1\rho}$ (Figure 5D). It was likely that the subject had involuntary motions during lengthy data acquisitions, and the blurring images were further degraded during the complex coregistration processes in the conventional approach.

As an internal reference method, the developed ARCADE mapping should alleviate any systematic errors known for both $R_2$ and $R_{1\rho}$ mappings due to different pulse sequence implementations on multiple platforms,[12,13] making it easier to standardize $R_2^a(\theta)$ measurement in a multicenter trial and be integrated in clinical studies. This new method is independent of the pulse sequence implementation as long as the image pixel intensities are spin-echo weighted, which is inherently insensitive to $B_0$ inhomogeneity. Advanced knee coil provides an excellent $B_1$ homogeneity, with less than ~5% variations in flip angle reported across the cartilage regions of interest in the sagittal plane.[35] Therefore, ARCADE could be reasonably considered to be insensitive to both $B_0$ and $B_1$ inhomogeneities. In short, an isotropic high-resolution 3D morphological and more relevant and sensitive $R_2^a(\theta)$ relaxation metric imaging could be foreseen with a single scan in a clinical setting[48,49] for both knee and other joints.

There are some limitations in the present work. First, only five knees were studied, and thus the reported statistical analysis might be biased. Second, the health status of collagen fibers (such as OA) at the MA locations could not be determined as the related residual dipolar interaction is nullified. However, it is possible to remedy this limitation by running an additional T2W sagittal scan with the knee rotated with a small angle along the left-right axis since the proposed method is efficient. Third, no in vivo validation against the "gold standard" of diffusion tensor imaging was performed. It has been demonstrated that diffusion tensor imaging could provide collagen alignment information in human knee cartilage.[50] $R_2^a(\theta)$ is mainly induced by restricted water molecular *rotational* diffusion within collagen fibers and the diffusion anisotropy derived from diffusion tensor imaging stems largely from water molecular *translational* diffusion along collagen fibers.[30,50] It would be interesting to compare how two different water diffusions can be associated with each other. Finally, the potential of the developed method in detecting the earliest cartilage changes that occur in OA might be diminished if GAG depletion is indeed to occur before disruption of the collagen network.

## 6 | CONCLUSIONS

We have developed an efficient method to measure the collagen orientation-dependent anisotropic transverse water proton relaxation rates in human knee cartilage. The potential to reduce clinical MR scan times significantly and derive more relevant and sensitive information on collagen integrity of both knee and other joints effectively warrants further evaluations and validations in larger clinical studies.

## ACKNOWLEDGMENTS

The authors are grateful to Drs. Yansong Zhao and Hui Wang from Philips Healthcare for support in optimizing T1ρ data acquisitions and James O'Connor and Suzan Lowe for help in collecting images.

## CONFLICT OF INTEREST

YP, RMPS and TLC are co-Inventors of an IP assigned to and managed by UMich.

## ORCID

*Yuxi Pang* https://orcid.org/0000-0001-5039-0236

## REFERENCES

1. Berendsen HJC. Nuclear magnetic resonance study of collagen hydration. *J Chem Phys*. 1962;36:3297–3305.
2. Fung BM. Orientation of water in striated frog muscle. *Science*. 1975;190:800–802.
3. Henkelman RM, Stanisz GJ, Kim JK, Bronskill MJ. Anisotropy of NMR properties of tissues. *Magn Reson Med*. 1994;32:592–601.
4. Sophia Fox AJ, Bedi A, Rodeo SA. The basic science of articular cartilage: structure, composition, and function. *Sports Health*. 2009;1:461–468.
5. Xia Y. Relaxation anisotropy in cartilage by NMR microscopy (muMRI) at 14-microm resolution. *Magn Reson Med*. 1998;39:941–949.
6. Grunder W. MRI assessment of cartilage ultrastructure. *NMR Biomed*. 2006;19:855–876.
7. Peto S, Gillis P. Fiber-to-field angle dependence of proton nuclear magnetic relaxation in collagen. *Magn Reson Imaging*. 1990;8:705–712.
8. Erickson SJ, Prost RW, Timins ME. The "magic angle" effect - background physics and clinical relevance. *Radiology*. 1993;188:23–25.
9. Hanninen N, Rautiainen J, Rieppo L, Saarakkala S, Nissi MJ. Orientation anisotropy of quantitative MRI relaxation parameters in ordered tissue. *Sci Rep*. 2017;7:9606.
10. Palmieri-Smith RM, Wojtys EM, Potter HG. Early Cartilage changes after anterior cruciate ligament injury: evaluation with imaging and serum biomarkers – a pilot study. *Arthroscopy*. 2016;32:1309–1318.
11. Link TM, Neumann J, Li X. Prestructural cartilage assessment using MRI. *J Magn Reson Imaging*. 2017;45:949–965.

12. Roemer FW, Kijowski R, Guermazi A. Editorial: from theory to practice – the challenges of compositional MRI in osteoarthritis research. *Osteoarthritis Cartilage*. 2017;25:1923–1925.
13. Link TM, Li X. Establishing compositional MRI of cartilage as a biomarker for clinical practice. *Osteoarthritis Cartilage*. 2018;26:1137–1139.
14. van Tiel J, Kotek G, Reijman M, et al. Is T1rho mapping an alternative to delayed gadolinium-enhanced MR imaging of cartilage in the assessment of sulphated glycosaminoglycan content in human osteoarthritic knees? An in vivo validation study. *Radiology*. 2016;279:523–531.
15. Shao H, Pauli C, Li S, et al. Magic angle effect plays a major role in both T1rho and T2 relaxation in articular cartilage. *Osteoarthritis Cartilage*. 2017;25:2022–2030.
16. Pedoia V, Haefeli J, Morioka K, et al. MRI and biomechanics multidimensional data analysis reveals R2–R1rho as an early predictor of cartilage lesion progression in knee osteoarthritis. *J Magn Reson Imaging*. 2018;47:78–90.
17. Russell C, Pedoia V, Majumdar S, Consortium A-A. Composite metric R2–R1rho (1/T2 - 1/T1rho ) as a potential MR imaging biomarker associated with changes in pain after ACL reconstruction: a six-month follow-up. *J Orthop Res*. 2017;35:718–729.
18. Wang P, Block J, Gore JC. Chemical exchange in knee cartilage assessed by R1rho (1/T1rho) dispersion at 3T. *Magn Reson Imaging*. 2015;33:38–42.
19. Akella SV, Regatte RR, Wheaton AJ, Borthakur A, Reddy R. Reduction of residual dipolar interaction in cartilage by spin-lock technique. *Magn Reson Med*. 2004;52:1103–1109.
20. Gold GE, Han E, Stainsby J, Wright G, Brittain J, Beaulieu C. Musculoskeletal MRI at 3.0 T: relaxation times and image contrast. *AJR Am J Roentgenol*. 2004;183:343–351.
21. Mlynarik V, Szomolanyi P, Toffanin R, Vittur F, Trattnig S. Transverse relaxation mechanisms in articular cartilage. *J Magn Reson*. 2004;169:300–307.
22. Singh A, Haris M, Cai K, Kogan F, Hariharan H, Reddy R. High resolution T1rho mapping of in vivo human knee cartilage at 7T. *PLoS ONE*. 2014;9:e97486.
23. Wyatt C, Guha A, Venkatachari A, et al. Improved differentiation between knees with cartilage lesions and controls using 7T relaxation time mapping. *J Orthop Transl*. 2015;3:197–204.
24. Momot KI, Pope JM, Wellard RM. Anisotropy of spin relaxation of water protons in cartilage and tendon. *NMR Biomed*. 2010;23:313–324.
25. Singh A, Haris M, Cai K, et al. Chemical exchange saturation transfer magnetic resonance imaging of human knee cartilage at 3 T and 7 T. *Magn Reson Med*. 2012;68:588–594.
26. Pang Y, Palmieri-Smith RM, Chenevert TL. A composite metric R2–R1 ρ measures an incomplete anisotropic R2 of human femoral cartilage at 3T. In Proceedings of the 26th Annual Meeting of ISMRM, Paris, France, 2018. (abstract 3104).
27. Mononen ME, Tanska P, Isaksson H, Korhonen RK. A novel method to simulate the progression of collagen degeneration of cartilage in the knee: data from the Osteoarthritis Initiative. *Sci Rep*. 2016;6:21415.
28. Eliav U, Navon G. A study of dipolar interactions and dynamic processes of water molecules in tendon by 1H and 2H homonuclear and heteronuclear multiple-quantum-filtered NMR spectroscopy. *J Magn Reson*. 1999;137:295–310.
29. Woessner DE, Snowden Jr BS. Magnetic relaxation under hindered rotation in fluids. *Advan Mol Relaxation Processes*. 1972;3:181–197.
30. Tourell MC, Momot KI. Molecular dynamics of a hydrated collagen peptide: Insights into rotational motion and residence times of single-water bridges in collagen. *J Phys Chem B*. 2016;120:12432–12443.
31. Woessner DE. Nuclear magnetic relaxation and structure in aqueous heterogenous systems. *Mol Phys*. 1977;34:899–920.
32. Xia Y. Magic-angle effect in magnetic resonance imaging of articular cartilage: a review. *Invest Radiol*. 2000;35:602–621.
33. Jordan CD, Saranathan M, Bangerter NK, Hargreaves BA, Gold GE. Musculoskeletal MRI at 3.0 T and 7.0 T: a comparison of relaxation times and image contrast. *Eur J Radiol*. 2013;82: 734–739.
34. Jones GP. Spin-lattice relaxation in the rotating frame: weak-collision case. *Phys Rev*. 1966;148:332–335.
35. Wang L, Schweitzer ME, Padua A, Regatte RR. Rapid 3D-T1 mapping of cartilage with variable flip angle and parallel imaging at 3.0T. *J Magn Reson Imaging*. 2008;27:154–161.
36. Berberat JE, Nissi MJ, Jurvelin JS, Nieminen MT. Assessment of interstitial water content of articular cartilage with T1 relaxation. *Magn Reson Imaging*. 2009;27:727–732.
37. Wang L, Regatte RR. $T_1\rho$ MRI of human musculoskeletal system. *J Magn Reson Imaging*. 2015;41:586–600.
38. Li X, Han ET, Busse RF, Majumdar S. In vivo $T_1\rho$ mapping in cartilage using 3D magnetization-prepared angle-modulated partitioned k-space spoiled gradient echo snapshots (3D MAPSS). *Magn Reson Med*. 2008;59:298–307.
39. Klein S, Staring M, Murphy K, Viergever MA, Pluim JPW. elastix: A Toolbox for Intensity-Based Medical Image Registration. *IEEE Trans Med Imaging*. 2010;29:196–205.
40. Bron EE, van Tiel J, Smit H, et al. Image registration improves human knee cartilage T1 mapping with delayed gadolinium-enhanced MRI of cartilage (dGEMRIC). *Eur Radiol*. 2013;23:246–252.
41. Yushkevich PA, Piven J, Hazlett HC, et al. User-guided 3D active contour segmentation of anatomical structures: significantly improved efficiency and reliability. *NeuroImage*. 2006;31: 1116–1128.
42. Kaneko Y, Nozaki T, Yu H, et al. Normal T2 map profile of the entire femoral cartilage using an angle/layer-dependent approach. *J Magn Reson Imaging*. 2015;42:1507–1516.
43. Monk AP, Choji K, O'Connor JJ, Goodfellow JW, Murray DW. The shape of the distal femur: a geometrical study using MRI. *Bone Joint J*. 2014;96-B:1623–1630.
44. Markwardt CB. Non-linear least-squares fitting in IDL with MPFIT. In Astronomical Data Analysis Software and Systems XVIII ASP Conference Series. 2009:411:251.
45. Friendly M, Monette G, Fox J. Elliptical insights: understanding statistical methods through elliptical geometry. *Stat Sci*. 2013;28:1–39.
46. Goodwin DW, Wadghiri YZ, Dunn JF. Micro-imaging of articular cartilage: T2, proton density, and the magic angle effect. *Acad Radiol*. 1998;5:790–798.
47. Matzat SJ, McWalter EJ, Kogan F, Chen W, Gold GE. T2 Relaxation time quantitation differs between pulse sequences in articular cartilage. *J Magn Reson Imaging*. 2015;42:105–113.

48. Heule R, Ganter C, Bieri O. Rapid estimation of cartilage T2 with reduced T1 sensitivity using double echo steady state imaging. *Magn Reson Med*. 2014;71:1137–1143.
49. Colotti R, Omoumi P, Bonanno G, Ledoux JB, van Heeswijk RB. Isotropic three-dimensional T2 mapping of knee cartilage: Development and validation. *J Magn Reson Imaging*. 2018;47:362–371.
50. Raya JG. Techniques and applications of in vivo diffusion imaging of articular cartilage. *J Magn Reson Imaging*. 2015;41:1487–1504.

**How to cite this article:** Pang Y, Palmieri-Smith RM, Malyarenko DI, Swanson SD, Chenevert TL. A unique anisotropic $R_2$ of collagen degeneration (ARCADE) mapping as an efficient alternative to composite relaxation metric ($R_2$-$R_{1\rho}$) in human knee cartilage study. *Magn Reson Med*. 2019;81:3763–3774. https://doi.org/10.1002/mrm.27621